Experimental and analytical studies on one-way concrete slabs reinforced with GFRP molded gratings

Shokrieh Mahmood Mehrdad* and Heidari-Rarani Mohammad

*Composites Research Laboratory, Department of Mechanical Engineering,
Iran University of Science and Technology (IUST), Narmak, Tehran 16844, Iran*

Abstract. Corrosion of steel rebars in bridge decks which are faced to harsh conditions, is a common problem in construction industries due to the porosity of concrete. In this research, the behavior of one-way concrete slabs reinforced with Glass fiber reinforced polymer (GFRP) molded grating is investigated both theoretically and experimentally. In the analytical method, a closed-form solution for load-deflection behavior of a slab under four-point bending condition is developed by considering a concrete slab as an orthotropic plate and defining stiffness coefficients in principal directions. The available formulation for concrete reinforced with steel is expanded for concrete reinforced with GFRP molded grating to predict ultimate failure load. In finite element modeling, an exact nonlinear behavior of concrete along with a 3-D failure criterion for cracking and crushing are considered in order to estimate the ultimate failure load and the initial cracking load. Eight concrete slabs reinforced with steel and GFRP grating in various thicknesses are also tested to verify the results. The obtained results from the models and experiments are relatively satisfactory.

Keywords: concrete slab; molded grating; FEM; analytical solution; experiment.

1. Introduction

In recent years, research on FRP composite grids has demonstrated that these products prone to be practical and cost-effective materials in various industrial applications. GFRP molded gratings become more desirable due to their properties such as corrosion resistant, fire retardant, maintenance free, lightweight, easy to install, uniform appearance, easy to fabricate, impact resistant, non-conductive, bidirectional load bearing, and cost effective make (Biddah 2006). The application of advanced composite materials in civil engineering has been evolving slowly due to economic reasons. Furthermore, the replacement of elements in conventional structural systems by composite materials has shown that it is difficult to justify the use of these materials structurally because of their different properties with respect to that of steel. There are fundamental differences between steel and FRP reinforcements; the latter has a lower modulus of elasticity and linear stress–strain diagram up to rupture, with no discernible yield point and different bond strength according to the type of FRP product. Therefore, researchers attempt to combine these materials with concrete to improve its properties. For example, GFRP rods have been used as reinforcement in the concrete or FRP laminates

---

* Corresponding Author, Email: shokrieh@iust.ac.ir

are currently used for external reinforcement of concrete beams and slabs.

Bank and Xi (1993) tested several concrete slabs reinforced with I and T shape pultruded gratings and considered failure modes, crack pattern and the bending behavior. Bank, *et al.* (1992, 1997) tested some concrete slabs reinforced with two different kinds of gratings that are used for a bridge deck. Hall and Mottram (1998) studied the behavior of twelve concrete beams reinforced with FRP panels placed in tension. Biddah (2006) studied the behavior of one-way concrete slabs reinforced with FRP pultruded (not molded) gratings, having different shear span-to-depth ratio. Capozucca (2007) analyzed the experimental flexural behavior of a concrete beam grid reinforced with CFRP bars. The experimental model is compared with both elastic theory of orthotropic plate and a FEM code. Tavarez, *et al.* (2003) studied the behavior of FRP composite grid reinforced concrete beams subjected to four-point bending, using LS-DYNA; an explicit finite element software. Ehab, *et al.* (2005) investigated a two-span girder type bridge using GFRP composite bars as reinforcement for the concrete deck slab. They have a comparison between GFRP and steel bars under identical service and environmental conditions. Eldib, *et al.* (2008) analyzed the ultimate behavior of two-way composite slabs using a software package of COSMOS. Non-linear material properties are considered. They validate the proposed finite element model by making a comparison with full-scale tests published in literature for one and two-way composite slabs.

As mentioned above, different kinds of grids, mostly pultruded grids are used by various researchers. GFRP molded gratings are more interesting to be used as reinforcements in concrete because of good bidirectional mechanical properties in contrast to pultruded ones that only have one directional property. The main purpose of this study is investigating the performance of a novel system, GFRP molded grating, as replacement for steel reinforcements, by considering equivalent axial rigidity $((EA)_{steel} = (EA)_{Grating})$. GFRP Molded grating itself has low modulus of elasticity, which causes to limit its loading range. Stiffness and ultimate failure load for definite maximum deflection will increase significantly by adding a layer of concrete on a grating. In other words, the added concrete will increase slab thickness, satisfies allowable deflection of concrete slab reinforced with steel. The proposed reinforcement approach is practical by considering lateral advantages like easy installation, high durability, easy transportation and especially high corrosion resistance of GFRP gratings. The presence of shrinkage and flexural cracks allows intrusion of the salt-laden condensation, contaminated rainwater, oxygen, and carbon dioxide gases. This mixture of chemicals and moisture eventually penetrates to the level of steel reinforcements and accelerates the corrosion rates.

2. FRP molded grating description

Lattices of rigidly connected ribs, known as grid structures have many advantages over the traditional construction methods, which use panels, sandwich cores and/or expensive framework (Huybrechts and Tsai 1996). Molded fiberglass grating is a composite of fiberglass reinforcements and a thermosetting resin system that is mostly produced by open or closed mold process. Compression-molded FRP gratings offer the best available combination of strength, durability and ease of installation. The matched-die process uniformly exerts over 600-tons of heated force throughout the entire glass and resin bonding operation. The hydraulic pressure of compression-molding forces glass deep into the resin and creates an extra dense and less porous grating than with open molded grating.

Molded fiberglass grating has equal strength in both directions and is made with square or rectangular grid patterns. Since it was developed much earlier than pultruded grating, it is widely used and

performs well in many applications. It is also a strong mesh grating panel, which allows efficient on-site cutting to minimize grating waste, and is significantly lighter in weight than metallic gratings. Percentage of glass (by weight) shall not exceed 35% so as to achieve maximum corrosion resistance, and to maintain the structural requirements of the contract. After molding, no dry glass fibers shall be visible on any surface of bearing bars or cross bars. All bars shall be smooth and uniform with no evidence of fiber orientation irregularities, interlaminar voids, porosity, resin rich or resin starved areas. The high resin content (65%) provides long maintenance free performance (Fibergrate website 2006). The molded grating used in this research, with square mesh 31 × 31 mm and 38 mm depth, is shown in Fig. 1.

3. Research significance

This paper includes three main parts: analytical investigation, finite element modeling and experimental work. In analytical section, load-deflection behavior, ultimate flexural capacity and ultimate shear capacity are discussed for a concrete slab reinforced with FRP grids. In finite element section, the use of advanced numerical simulation is described for the analysis of FRP reinforced concrete. Crack initiation load, ultimate capacity load and crack patterns are estimated by considering aspects of nonlinear behavior of reinforced concrete such as tension softening and shear transfer coefficient. The failure criterion for concrete due to a multi-axial stress state is based on the method proposed by William and Warnke. This research also presents experimental results of two GFRP grating and eight one-way concrete slabs; including six reinforced with GFRP grating and two with steel reinforcement. The behavior of concrete slabs reinforced with GFRP gratings is compared with the behavior of a slab reinforced with steel reinforcements. The information throughout this research is useful for future field applications and development of design guidelines for one-way concrete slabs reinforced with GFRP molded grating.

4. Experimental procedure

The proposed work focused on replacing steel reinforcement of concrete slabs by GFRP molded grating. Hence, the objective of the test program is to investigate the performance of GFRP grating reinforced concrete members in bending test up to failure. The test observations include concrete
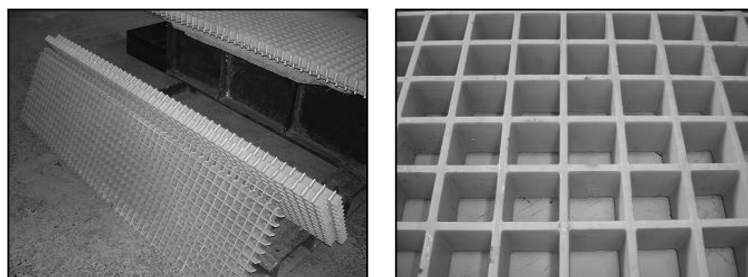

Fig. 1 Overview of GFRP molded grating reinforcement

behavior at cracking, crack pattern, deflection, ultimate capacity, and failure mode. For this purpose, two molded gratings are first tested under four-line bending. Eight one-way concrete slabs, including six reinforced with GFRP grating and two with steel reinforcement, are then constructed and tested. The side view of the composite slab section is depicted in Fig. 2.

4.1 Test specimens and setup

Eight medium scale specimens are constructed and tested. The overall length and width of the slabs are 1800 mm and 450 mm, respectively. The specimens are tested in four-point bending over a 1650 mm simply supported span which kept constant throughout the study. Specimens G1 and G2 are single molded gratings without any concrete with the same 1800 × 450 mm dimensions. Specimens SG3 to SG8 are concrete slabs reinforced with similar molded gratings in the tension zone and various thicknesses. The first two specimens have 80 mm thickness. SG5 and SG6 have 120 mm thickness. SG7 and SG8 have 150 mm thickness. Slabs SS9 and SS10 have the same dimensions as slabs SG3 and SG4 but reinforced with conventional steel rebars (12 mm diameter) as the mesh reinforcement with the same longitudinal and transverse spacing of 90 mm. Fig. 3 shows the dimensions, loading and supporting system of the specimens. Each slab instrumented by four dial gauges to record deflections of slabs during the testing. The maximum deflection of slabs was recorded on two points at mid-span along the slab width by using two dial gauges. The load was monotonically applied to the slab at a rate of 5 kN/min, under load control, by means of one MTS-150-kN hydraulic jack. The test set-up of specimen G1 and SG3 are shown in Fig. 4. The loading is continued up to final failure of specimen. During the tests, the slabs are carefully inspected and crack propagation through different load stages are marked with a chalk.

4.2 Material properties

The reinforcing steel rebars used in this research are of yield strength 410 MPa and the weight of the
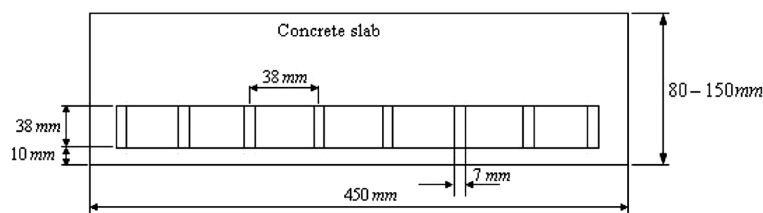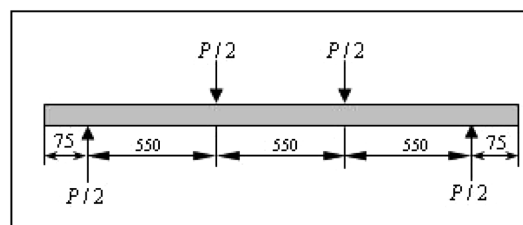

Fig. 2 Cross-section of the proposed slab

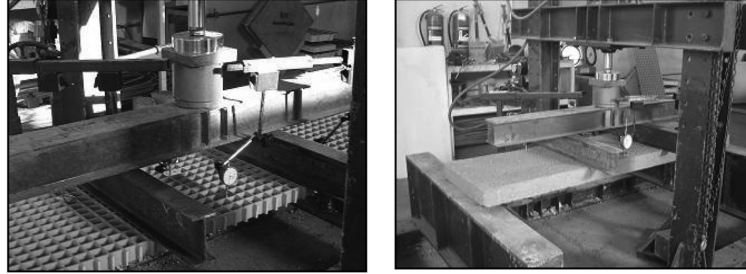Fig. 3 Loading, dimension and supporting system (dimensions in mm)

Fig. 4-Test set-up of specimen G1 and SG3 (left and right respectively)

steel mesh reinforcement is 15.8 kg. The grating flexural modulus of elasticity in the fiber direction is 30.5 GPa, and its weight is 15.6 kg. The average concrete cylinder compressive strength is 19.7 MPa. This was obtained from the 28-day strength of cylindrical and cubic samples. It should be also mentioned that authors selected a relatively low class of concrete because it is commonly used in practice in Iran and they wanted to know effect of GFRP grids on concrete slabs.

5. Analytical investigation

5.1 Load-deflection behavior

Considering a concrete slab as an orthotropic plate, the deflection equation can be expressed as (Capozucca 2007, Ugural 1981):

$$D_{xx}\frac{\partial^4 w}{\partial^4 x} + 2H\frac{\partial^4 w}{\partial^2 x \partial^2 y} + D_{yy}\frac{\partial^4 w}{\partial^4 y} = P(x, y) \tag{1}$$

where D_{xx} and D_{yy} are flexural rigidity in x and y direction, respectively and $H = D_{xy} + 2D_s$. For a concrete slab $D_s = 0$ and other coefficients are defined as below (Ugural 1981):

$$D_{xx} = \frac{E_c}{1 - v_c^2}\left(I_{cx} + \left(\frac{E_c}{E_s} - 1\right)I_{sx}\right) \tag{2}$$

$$D_{yy} = \frac{E_c}{1 - v_c^2}\left(I_{cy} + \left(\frac{E_c}{E_s} - 1\right)I_{sy}\right) \tag{3}$$

$$D_{xy} = v_c\sqrt{D_{xx}D_{yy}} \tag{4}$$

where I_{cx} and I_{sx} are moments of inertia of concrete and reinforcement in the cross-section perpendicular to $x = cte$ ($x = cte$, means x is constant), respectively. I_{cy} and I_{sy} are moments of inertia of the concrete and the reinforcement in the cross-section perpendicular to $y = cte$, respectively. E_c and E_s

are modulus of elasticity of the concrete and the reinforcement, respectively.

In Eqs. (2) and (3), the moment of inertia strongly depends on the neutral axis of the section. Assuming concrete crushing before yielding of reinforcements and considering Whitney stress block (Macginley and Chao 1990), a can be obtained from Eq. (5).

$$\frac{0.85f_c' \, bd}{A_{FRP}E_{FRP}\varepsilon_{cu}}a^2 + da - 0.85d^2 = 0 \tag{5}$$

where $c = \dfrac{a}{0.85}$ is neutral axis depth, b is slab width, d is effective depth of slab, A_s is area of the tensile reinforcement (either steel rebars or gratings), ε_{cu} is ultimate compressive strain of concrete (0.003), and f_c' is ultimate compressive cylinder strength of the concrete.

According to Levy method (Ugural 1981), the solution of Eq. (1) includes homogenous and particular solutions, $w = w_h + w_p$. Due to simply supported boundary conditions, the homogenous solution (w_h) is considered as Fourier series, $w_h = \sum\limits_{m=1}^{\infty} f_m(y)\sin(m\pi x/l)$. Substitution of w_h in homogenous Eq. (1) result in $f_m(y)$ as below

$$f_m(y) = A_m \sinh(\alpha_m y) + B_m \cosh(\alpha_m y) + C_m y \sinh(\alpha_m y) + D_m y \cosh(\alpha_m y) \tag{6}$$

where $\alpha_m = \dfrac{m\pi}{l}\sqrt{\dfrac{H}{D_y}}$. To obtain particular solution, both $P(x,y)$ in Eq. (1) and w_p should be expanded in single Fourier series. Since the loading conditions is linear loading as shown in Fig. 5, for any arbitrary distance e.g. $x = x_1$, $P(x,y)$ can be written as $P(x,y) = \sum\limits_{m=1}^{\infty} P_m(y)\sin(m\pi x/l)$ where $P_m(y) = (2P_0/l)\sin(m\pi x_1/l)$.

Thus, particular solution obtained as $w_p = (2P_0 l^3/D_x \pi^4)\sum\limits_{m=1}^{\infty}\dfrac{1}{m^4}\sin(m\pi x_1/l)\sin(m\pi x/l)$ where P_0 is the load intensity (N/m).

From the symmetric boundary conditions along the x direction, it can be concluded that A_m and D_m coefficients in Eq. (6) are zero. Finally, the load-deflection relation for a concrete slab with any
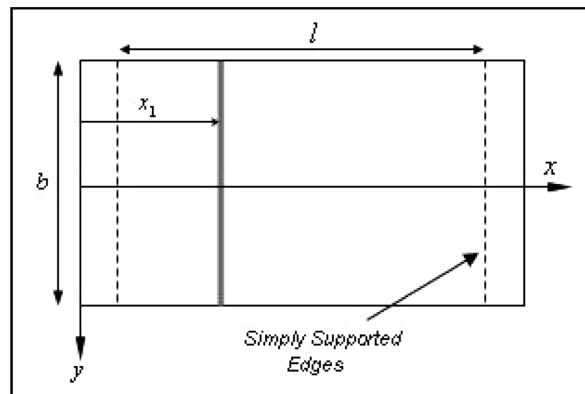

Fig. 5 Boundary and loading conditions of the rectangle plate

reinforcements can be expressed as:

$$w(x, y) = \sum_{m=1}^{\infty} \left[B_m \cosh(\alpha_m y) + C_m y \sinh(\alpha_m y) + \frac{2P_0 l^3 \sin(m\pi x_1/l)}{D_x m^4 \pi^4} \right] . Sin(m\pi x/l) \qquad (7)$$

B_m and C_m coefficients are obtained by applying the boundary conditions of free edges at $y = \pm b / 2$, in Eq. (7). At free edges bending moment and shear force should be equaled to zero as below

$$M_y = -\left(D_y \frac{\partial^2 w}{\partial y^2} + D_{xy} \frac{\partial^2 w}{\partial x^2} \right) = 0, \, Q_y = -\frac{\partial}{\partial y} \left(D_y \frac{\partial^2 w}{\partial y^2} + H \frac{\partial^2 w}{\partial x^2} \right) = 0 \qquad (8)$$

5.2 Ultimate flexural capacity

The stress distribution across the steel rebars is negligible as a result of their small dimensions relative to the concrete cross-section. Accordingly, the ultimate moment obtained from Whitney stress block (Biddah 2006, Macginley and Chao 1990) can be written as follows.

$$M_u = 0.85 f_c' ab(d - a/2) \qquad (9)$$

That for four-point bending conditions, the ultimate load is $F_u = (6/l) \times M_u$. On the other hand, by replacing the rebars by the pultruded gratings, it is necessary to consider the stress distribution across I-section. In other words, Eq. (9) must be revised as follows:

$$M_u = 0.85 f_c' ab(d - a/2) + \Delta M_u \qquad (10)$$

From Fig. 6, ΔM_u is obtained as follows

$$\Delta M_u = 0.85 f_c' ba(h/2 - \bar{y}) . \qquad (11)$$

where $\bar{y}$ is the centriod of the stress trapezoid across the reinforcement height.
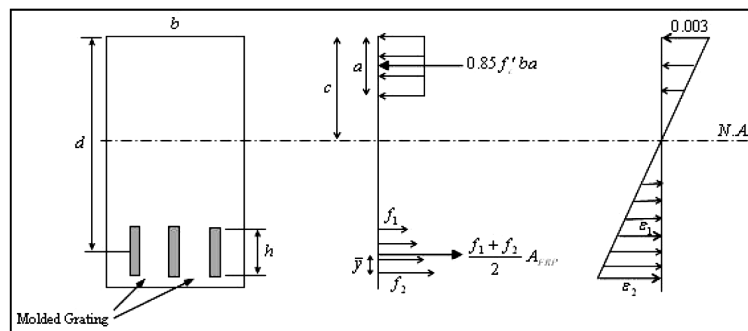

Fig. 6 Stress distribution at concrete slab section

$$\bar{y} = \frac{2f_1 + f_2}{f_1 + f_2} \times \frac{h}{3}, f_1 = E_s \varepsilon_1, f_2 = E_s \varepsilon_2. \tag{12}$$

By using the strain diagram and substituting for the strains in Eq. (12), $\bar{y}$ is obtained as:

$$\bar{y} = \frac{3}{2}\left(1 - \frac{h}{6(d-c)}\right). \tag{13}$$

5.3 Ultimate shear capacity

The shear behavior of reinforced concrete members is generally more complicated than the flexural behavior. Failure in shear takes place under combined stresses resulting from applied shear force and bending moment. According to the ACI-318 (ACI 318-99 1999), the shear strength of steel reinforced concrete members without shear reinforcement is given in SI units by:

$$V_c = \frac{1}{6}\left(\sqrt{f_c'} + 100\rho\frac{V_u d}{M_u}\right)b_w d \tag{14}$$

where V_c is the shear strength provided by the concrete, b_w is web width, d is the effective depth of the cross-section, ρ is ratio of tension reinforcement, V_u is factored shear force at section considered, M_u is factored moment at section considered. Based on the results in (Wegian and Abdalla 2005), Eq. (14) and other modified relations by different authors overestimate the ultimate shear capacity. Thus, Eq. (15) can be used to predict the ultimate shear capacity of FRP reinforced concrete members:

$$V_c = 2\left(f_c' \cdot \frac{\rho E_f}{E_s} \cdot \frac{d}{a}\right)^{1/3} b_w d \tag{15}$$

where a is shear span, E_f and E_s are elastic modulus of FRP reinforcement and elastic modulus of steel reinforcement, respectively.

6. Finite element modeling of full-size reinforced concrete slab

Nonlinear finite element analysis (FEA) can be used to numerically model the concrete behavior in order to confirm the analytical calculations, as well as to provide a valuable supplement to the laboratory investigations. Using an explicit finite element method, especially to model a quasi-static experiment as the one presented herein, can result in long run times due to the large number of time steps that are required. Finite element models are developed to simulate the behavior of four full-size slabs from linear to nonlinear responses and up to final failure, using ANSYS10 (ANSYS User's Manual 2003) software. Ideally, the bond strength between the concrete and steel reinforcement should be considered. However, in this study, perfect bond between materials is assumed. To provide perfect

bond, the beam element representing as the reinforcements is connected between the nodes of each adjacent concrete solid element, in such a way that the two materials shared the same nodes. The model is developed in ANSYS software work based on smeared crack models. It is capable of including the behavior of concrete in both tension and compression (cracking and crushing). All aspects of nonlinear behavior of reinforced concrete such as tension softening, shear transfer coefficient, and bilinear stress-strain relationships for steel are accounted for.

6.1 Element types

To simulate the effect of concrete, SOLID65 has been used. It is a 3-D isoperimetric element with eight nodes and three degrees of freedom at each node. The element is capable of plastic deformations, cracking in three orthogonal directions in tension, and crushing in compression. A BEAM188 element is used to model the steel and FRP reinforcements. Two nodes are required for this element and each node has three degrees of freedom. An eight-node solid element, Solid45, is also used for the steel plate at the supports in the slab model. This element is defined with eight nodes having three degrees of freedom at each node.

6.2 Material properties

Development of a model simulating the real behavior of concrete is a challenging task. Concrete is a quasi-brittle material and has different behavior in compression and tension (Kachlakev and Millaer 2001). Accordingly, the compressive uni-axial stress-strain relationship is simplified as in Fig. 7. The points shown in Fig. 7, assuming linear elastic behavior up to about 30 percent of the maximum compressive strength, are obtained from Eq. (16).

$$f = \frac{E_c \varepsilon}{1 + (\varepsilon/\varepsilon_0)^2}, \ \varepsilon_0 = \frac{2f_c'}{E_c}, E_c = \frac{f}{\varepsilon} \tag{16}$$
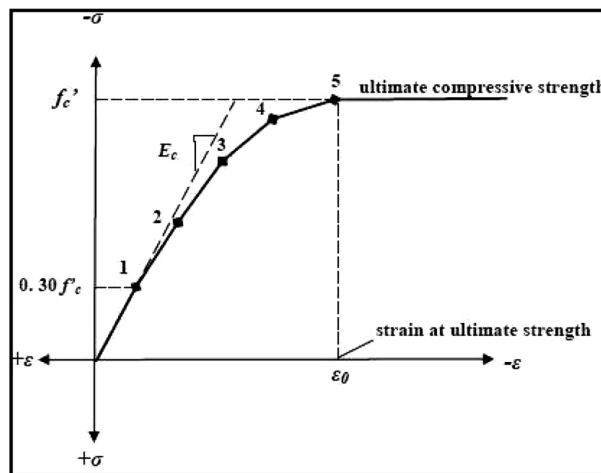

Fig. 7 Simplified compression uni-axial stress-strain curve for the concrete (Kachlakev 2001)

where f is stress at any strain ε, ε_0 is strain at the ultimate compressive cylinder strength f_c'.

To assess the FE results with experiment one, the real properties of concrete obtained from experiment was used in FE inputs. The concrete properties used in the FEM study are $v = 0.2$ and $f_c' = 200$, 178, 201, and 210 kg/cm^2 for SG3 (or SG4), SG5 (or SG6), SG7 (or SG8), and SS9 (or SS10), respectively. While v and f_c' are the Poisson's ratio and the compressive concrete cylinder strength, respectively. $E_c = 15800\sqrt{f_c'}$ and $f_t = 2\sqrt{f_c'}$ are the Young's modulus and the tensile strength of concrete in kg/cm^2 (ACI 318 1999).

The shear transfer coefficient, β_t, represents conditions of the crack face. For all elements, a shear transfer coefficient is introduced that represents a shear strength reduction factor for those subsequent loads that induce sliding (shear) across the crack face. If the crack closes, then all compressive stresses normal to the crack plane are transmitted across the crack and only a shear transfer coefficient for a closed crack is introduced. In software, the value of β_t ranges from 0 to 1, with 0 representing a smooth crack (complete loss of shear transfer) and 1 representing a rough crack (no loss of shear effect) (ANSYS User's Manual 2003). Since choosing the value of β_t affects convergence, the shear transfer coefficient used in this study is equal to 0.2. The steel in the FEM is assumed to be an elastic-perfectly plastic material with Poisson's ratio 0.3 and Young's modulus 200 GPa. The mechanical properties for gratings are also shown in Table 1.

6.3 Failure criteria for the concrete

Three-dimensional failure surfaces for concrete where both cracking and crushing failure are accounted for, are shown in Fig. 8. The most significant nonzero principle stresses are in x and y

Table 1 FEM inputs for molded grating properties (Tsai 1980 and Fibergrate 2006)

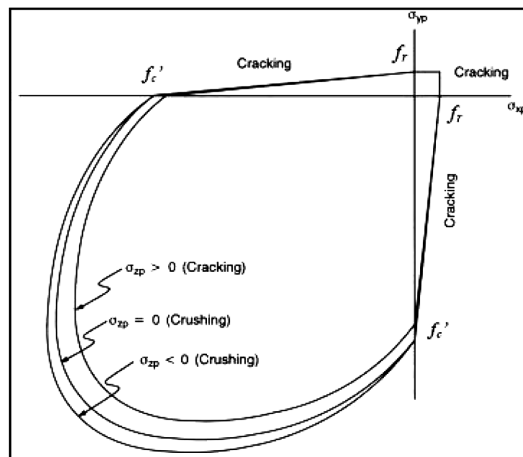| Elastic modulus, GPa	Shear modulus, GPa	Major Poisson's ratio	Tensile strength, MPa
$E_x = 30.5$	$G_{xy} = 4.14$	$v_{xy} = 0.26$	
$E_y = 30.5$	$G_{yz} = 4.14$	$v_{yz} = 0.26$	550
$E_z = 7.24$	$G_{xz} = 3.65$	$v_{xz} = 0.4$	

Fig. 8 3-D failure surfaces for concrete (Chen 1992 and Kachlakev 2001)

directions represented by σ_{xp} and σ_{yp}, respectively. In concrete element, cracking occurs when the principal tensile stress in any direction lays outside of the failure surface. Crushing occurs when all principal stresses are compressive and lie outside of the failure surface.

6.4 Loading and boundary conditions

The eight full-size slabs were tested in four-point bending as shown in Fig. 3. The finite element models were loaded at the same locations. A 5 mm thick steel plate, modeled using Solid45 elements, was added at each support's location in order to avoid stress concentration. Moreover, a single line support was placed under the centerline of each steel plate to allow rotation of the plate. Fig. 9(a) illustrates the steel plate at the support. In order to reduce the runtime of the analysis, a quarter of the slab is modeled. At the plane of symmetry, the displacement in the direction perpendicular to the plane is fixed. Fig. 9(b) shows the loading and symmetry conditions.

7. Comparison of theoritical and experimental results

A summary of the experimental results is presented in Table 2. This table includes the ultimate load (F_u), the maximum deflection (δ_{max}), and the initial cracking load (F_i). The theoretical ultimate load and maximum deflection are calculated from Eqs. (10) or (16), and (8), respectively.

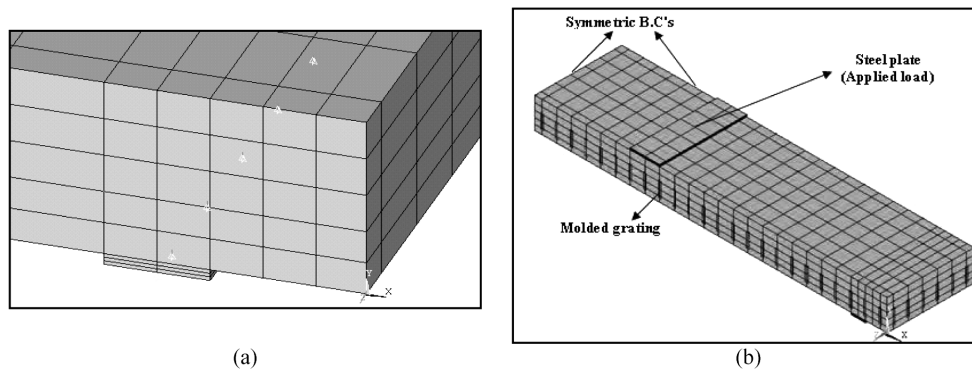The experimental results and the corresponding analytical calculations for ultimate load are reasonable.

Fig. 9 a) Steel plate with line support, b) Loading and boundary conditions

Table 2 Experimental, FEM and analytical results

Specimen	Theory		FEM			Experiment			Failure Modes, (Experiment)
	δ_{max}, mm	F_u, kN	δ_{max}, mm	F_u, kN	F_i, kN	δ_{max}, mm	F_u, kN	F_i, kN	
SG3, 4	52.2	29.7	46.16	24.87	5.87	48.75	26.55	6.87	Concrete crushing
SG5, 6	35.18	65.8	27.00	63.83	17.68	30.65	78.37	19.80	Shear bond failure
SG7, 8	18.4	112.17	17.60	85.00	33.60	21.65	99.00	36.85	Diagonal shear
SS9, 10	34.0	44.79	24.10	39.82	16.80	31.35	40.70	19.25	Concrete crushing

The reason for differences between maximum deflections is that the extended equations in this study are applicable only for the elastic region, whereas the deflections in the experimental results are reported for both linear and non-linear regions. In all concrete specimens, neglecting micro-cracks near support, the primary flexural cracks are seen at the mid-span area (Figs. 10 and 11). The progress of the cracks that is seen in Fig. 11(a) shows a fairly regular crack pattern. In the FEM, a smeared cracking approach is used. In this approach, cracking of the concrete occurs when the principal tensile stress exceeds the ultimate tensile strength. The elastic modulus of the material is then assumed to be zero in the direction parallel to the principal tensile stress direction (Kachlakev and Millaer 2001). Concrete cracking in various load steps for SG3 specimen is shown in Fig. 10.

The SG3, SG4, SS9, and SS10 specimens failed by concrete crushing. The flexural capacity of SG3 and SG4 was less than that of SS9 and SS10. The failure of SG3 and SS10 are shown in Fig. 11(a) and (b), respectively. The mode of failure is completely different in both cases. In the slab reinforced with GFRP grid, failure is planar due to the distribution of stresses by the grating, whereas the failure in the slab reinforced with steel grid is local. Fig. 11 (a) and (b) shows various crack patterns for different
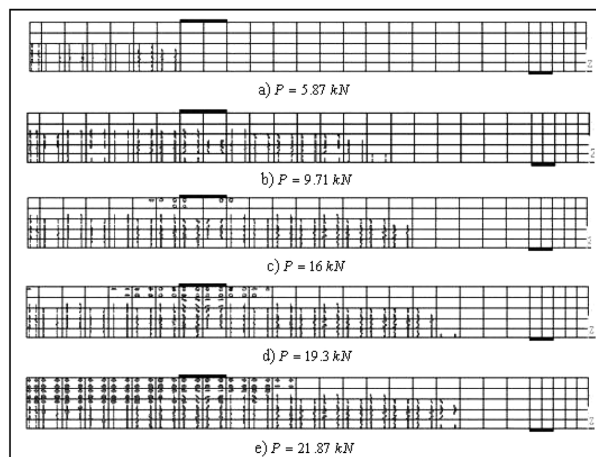

a) $P = 5.87\ kN$

b) $P = 9.71\ kN$

c) $P = 16\ kN$

d) $P = 19.3\ kN$

e) $P = 21.87\ kN$

Fig. 10 Concrete cracking in a quarter of slab at various loads

(a) SG3   (b) SS10

Fig. 11 Failure of specimen SG3 and SS10

reinforcements. Crack spacing is almost equal to FRP grid spacing because the grid spacing strongly influenced the crack spacing and width. Crack pattern also depends on the bond quality between reinforcement and concrete. This bonding is so weak for FRP grid rather than steel reinforcement. So, transverse bars play an anchorage role for longitudinal bars. Tests showed that the longitudinal steel rebars, unlike longitudinal bars in FRP grid, transfer stress to concrete continuously due to strong bond and cracks occurred at locations where transferred shear stress from longitudinal bar exceeded the bond strength of concrete and reinforcement.

In specimens SG5 and SG6 or SG7 and SG8, the failure mode changed from flexural to shear. The failure of concrete-encased composite member generally involves two possible failure modes; the shear bond failure and diagonal shear failure (Biddah 2006). Fig. 12(a) shows that the failure in SG5 is of the second type. A molded grating was also tested under four point bending to estimate the ultimate failure load. Fig. 12(b) illustrates the deflection of the molded grating. Finally, 137 kN load is applied without final failure observation.

The applied load versus central-deflection of the concrete slabs is presented in Fig. 13. Due to the low elastic modulus of the molded fiber glass grating in comparison with steel, bigger deflection and lower crack initiation load were observed for the concrete slabs reinforced with molded gratings. As can be seen from Figs. 11 and 12, cracks in SS10 are wider than primary cracks in SG3. The balanced reinforcement ratio, ρ_b, is obtained by applying the equilibrium and compability conditions and using the equivalent rectangular stress block by (Wegian and Abdalla 2005)

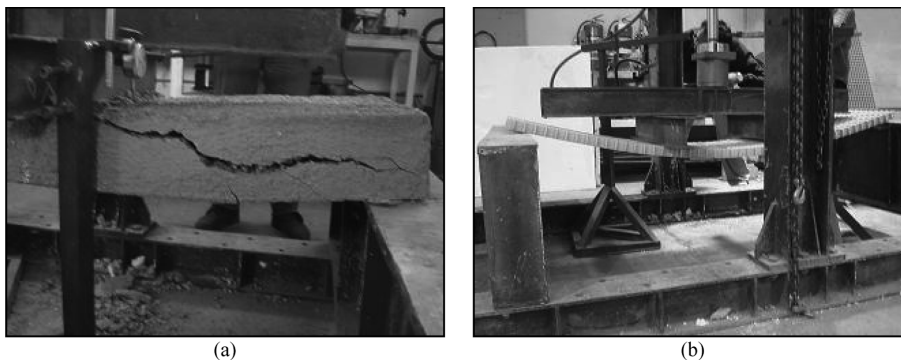(a)   (b)

Fig. 12 a) Failure of specimen SG5, b) Deflection of molded grating

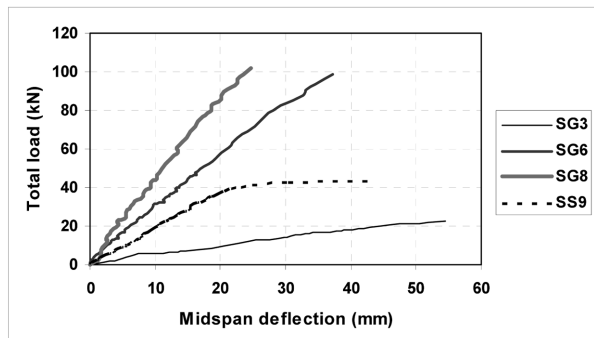Fig. 13 Load-deflection behavior of specimens SG3, SG6, SG8 and SS9

$$\rho_b = \frac{0.85\beta_1 f_c'}{f_u}\left(\frac{0.003E_f}{0.003E_f + f_u}\right) \tag{17}$$

where f_u is rupture stress of FRP reinforcement and β_1 is ratio of depth of equivalent rectangular stress block to depth of neutral axis. The balanced reinforcement ratios for the concrete sections reinforced with molded grating and steel reinforcements are 0.37% and 2.05%, respectively. These values show that the balanced reinforcement ratios for FRP reinforced concrete sections are lower than those for steel reinforced concrete sections. This is due to the higher tensile strength and the lower modulus of elasticity of the FRP reinforcement relative to the conventional steel. For practical ratios of FRP reinforcement, FRP reinforced concrete sections are designed as over-reinforced sections (Wegian and Abdalla 2005) in order to control the deflection and cracking, and to avoid the rupture of the FRP bars. Thus, the strength and stiffness of the slabs increase with the increase in the slab thickness having the same GFRP molded grating.

8. Conclusions

Experimental and analytical studies are performed on the behavior of concrete slabs reinforced with GFRP molded gratings. In analytical proposed method, a slab concrete is considered as an orthotropic plate and its load-deflection is predicted in a four-point bending conditions. The available formulation for steel reinforced concrete members is modified to use for reinforced concrete slabs with GFRP molded gratings. In finite element analysis, a 3-D failure criterion, instead of common Drager-Prager criterion, and a nonlinear behavior of concrete are employed in an attempt to present a model capable of predicting the initial cracking load, ultimate failure load and cracking patterns with more accuracy. Six slabs are reinforced by GFRP grids and two slabs are reinforced by steel rebars in grid shape. Three variables, i.e., slab depth, reinforcement type, and the reinforcement without any concrete are considered. The following observation can be concluded:

(1) Comparison of results show theoretical and FEM data are in a relatively good agreement with the experimental one. The results of the theoretical model in comparison with the FE results, overestimate the ultimate capacity load. That is why in the analytical model the behavior of concrete and grating is supposed to be perfectly elastic.

(2) The flexural and shear strength of slabs reinforced with GFRP gratings (i.e. SG3, 4) are lower than those of steel reinforced slabs (i.e. SS9, 10) due to the reduced compression stress block and also the nature of cracking (From comparison between slabs with same dimensions).

(3) In the slabs reinforced with GFRP molded gratings, failure is completely different from those reinforced with steel reinforcements. The locally damage is observed in SS9, and SS10, whereas the failure region in SG3, and SG4 due to more uniformly stress distribution is more global. For FRP grid reinforcements, transverse bars play two roles: anchorage of longitudinal bars and controlling the crack. Cracks follow a regular pattern during the tests that it shows the grid spacing strongly influenced the crack spacing and width.

(4) From Fig. 13, deflections and strains of concrete members (in same dimension) reinforced with FRP gratings are generally higher than those reinforced with steel rebar mesh. The deflection of the slab is a function of reinforcement stiffness and actual reinforcement ratio used in the slab. FRP reinforced slabs, especially with smaller reinforcement ratio, exhibit adequate warning prior to failure

through relatively large deflections and crack widths.

(5) The strength and stiffness of the slabs increase with increasing of the slab thickness reinforced with the same molded gratings. From the reported results, by increasing 4 cm slab thickness (specimens SG5 and SG6), the initial crack load is the same as the load for specimens SG3, SG4, whereas ultimate load increases 1.93 times. Also, for specimens SG7, SG8 the initial cracking load and ultimate failure load increase 1.91 and 2.43 times compared with specimens SG3, SG4.

(6) According to experimental results, this type of GFRP grid is not useful to reinforce slabs with low thickness because of high flexural strength as well as low flexural stiffness of grid. Therefore, the close agreement in flexural behavior between slabs SG3 and SG8 shows that GFRP reinforced slabs should be over-reinforced with an equivalent flexural tension stiffness of reinforcement to steel.

Eventually, with further research and development, slabs made of concrete and GFRP molded grating reinforcements can potentially offer an alternative for bridge deck slab construction. GFRP grids are stiff, high strength, high corrosion resistance, and also easily to be installed which could economically result in an alternative solution for construction instead of traditional methods. The information provided throughout this research could be useful in establishing design guidelines for structures reinforced with GFRP gratings.

Acknowledgments

References

ACI 318-99 (1999), *Building Code Requirements for Reinforced Concrete,* American Concrete Institute, Farmington Hills, Michigan.

ANSYS User's Manual Revision 10 (2003), ANSYS Inc., Canonsburg, Pennsylvania.

Bank, L.C., Xi, Z. and Muley, E. (1992), "Tests of Full-Size Pultruded FRP Grating Reinforced Concrete Bridge Decks", *Conf. Proc. of ASCE-Materials Engineering congress*, New York, 618-631.

Bank, L.C., Frosting, Y. and Shapira, A. (1997), "Three-Dimensional FRP Grating Cages for Concrete Beams", *ACI Struct. J.*, **94**(6), 643-652.

Bank, L.C. and Xi, Z. (1993), "Pultruded FRP Grating Reinforced Concrete Slabs", *In Fiber-Reinforced-Plastic for Concrete Structures-Int. Symposium*, SP-138, American Concrete Institute, 561-583.

Biddah, A. (2006), "Structural Reinforcement of Bridge Decks Using Pultruded GFRP Grating", *Compos. Struct.*, **74**(1), 80-88.

Capozucca, R. (2007), "Analysis of the Experimental Flexural Behavior of a Concrete Beam Grid Reinforced With CFRP Bars", *Compos. Struct.*, **79**(4), 517-526.

Chen, W.F. (1992), *Plasticity in Reinforced Concrete*, McGraw-Hill, USA.

Ehab, E., Brahim, B., Amr, E. and Dominique, N. (2005), "Field Investigation on the First Bridge Deck Slab Reinforced with Glass FRP Bars Constructed in Canada", *J. Compos. Constr.*, **9**(6), 470-479.

Eldib, M.E.A.H., Maaly, H.M., Beshay, A.W. and Tolba, M.T. (2008), "Modeling and analysis of two-way composite slabs", *J. Constr. Steel Res.*, **9**(5), 1236-1248.

Fibergrate website (2006), www.fibergrate.com.

Hall, J.E. and Mottram, J.T. (1998), "Combined FRP Reinforced and Permanent Formwork for Concrete Members", *J. Compos. Constr.*, **2**(2), 78-86.

Huybrechts, S. and Tsai, S.W. (1996), "Analysis and Behavior of Grid Structures", *Compos. Sci. Technol.*, **56**(9), 1001-1015.

Kachlakev, D. and Millaer, T. (2001), "Finite Element Modeling of Reinforced Concrete Structures Strengthened with FRP Laminates", Report for Federal Highway Administration, Washington, 5-23.

Macginley, T.J. and Choo, B.S. (1990), *Reinforced Concrete: Design Theory and Examples*, Taylor & Francis, London.

Tavarez, F.A., Bank, L.C. and Plesha, M.E. (2003), "Analysis of Fiber-Reinforced Polymer Composite Grid Reinforced Concrete Beams", *ACI Struct. J.*, **100**(2), 250-258.

Tsai, S.W. and Hahn, H.T. (1980), *Introduction to Composite Materials*, Technomic Publishing Co., Westport.

Ugural, A.C. (1981), *Stresses in Plates and Shells*, McGraw-Hill, New York.

Wegian, F.M. and Abdalla, H.A. (2005), "Shear Capacity of Concrete Beams Reinforced with Fiber Reinforced Polymers", *Compos. Struct.*, **71**(1), 130-138.

CC

Notations

a	= depth of Whitney stress block
b	= width of slab
w	= deflection of plate
D_{xx}	= flexural rigidity in x direction
D_{yy}	= flexural rigidity in y direction
D_{xy}	= torsional rigidity
I_{cx} and I_{sx}	= moment of inertia of concrete and reinforcement in cross-section perpendicular to, $x = cte$ respectively (*cte* is the abbreviation of constant).
I_{cy} and I_{sy}	= moment of inertia of the concrete and the reinforcement in cross-section perpendicular $y = cte$, respectively.
$c = \dfrac{a}{0.85}$	= neutral axis depth
b	= slab width
d	= effective depth
A_s	= area of the tensile reinforcement either steel rebars or gratings
ε_{cu}	= ultimate strain of concrete, (0.003).
f_c'	= the ultimate compressive strength of the concrete
P_0	= load intensity (N/m)
$\bar{y}$	= centriod of stress trapezoid at the reinforcement area
M_u	= ultimate moment
f	= stress at any strain ε
ε_0	= strain at the ultimate compressive strength f_c'
β_t	= shear transfer coefficient
σ_{xp} and σ_{yp}	= principal stresses in x and y direction respectively
F_u	= ultimate failure load
δ_{max}	= maximum deflection
F_i	= initial cracking load